Green Chemistry

PAPER

View Article Online
View Journal | View Issue

Cite this: *Green Chem.*, 2026, **28**, 351

Lithium extraction from spinel $LiMn_2O_4$ with simultaneous preparation of λ-MnO_2 under mild conditions using sodium hypochlorite

Yanhui Kong, [a] Yutaro Takaya, [b,d] Mauricio Córdova-Udaeta [c] and Chiharu Tokoro *[b,d]

Lithium extraction from spinel $LiMn_2O_4$ is of significant importance, because it serves not only as one of the mainstream cathode materials for lithium-ion batteries (LIBs) but also as a crucial precursor for the preparation of isostructural λ-MnO_2 (delithiated $LiMn_2O_4$), widely used in the selective lithium extraction from brines and seawater. This study proposes a novel approach for lithium extraction from $LiMn_2O_4$ that preserves the structural integrity of the spinel during delithiation, by using sodium hypochlorite (NaClO) as an oxidant under comparatively mild conditions (room temperature, weakly acidic environment). At pH = 4, approximately 99.3% of lithium was selectively extracted without detectable Mn loss. Mechanistic analysis revealed that the process primarily involves Mn^{3+} oxidation to Mn^{4+}, with a minor contribution from H^+/Li^+ ion exchange. The resulting λ-MnO_2 maintained its spinel morphology and exhibited good lithium uptake capacity and cyclic performance. Moreover, life cycle and techno-economic assessments demonstrate that the NaClO-based oxidative selective delithiation route offers significantly lower environmental impacts, energy consumption, and overall cost than the previously reported $Na_2S_2O_8$-based oxidation process. Compared with traditional acid leaching, it demonstrates advantages in terms of human toxicity and freshwater aquatic ecotoxicity, and also offers superior λ-MnO_2 yield and downstream processing owing to its higher lithium selectivity and negligible Mn loss. This work provides a simple, efficient, and sustainable strategy for λ-MnO_2 preparation and holds promise for the selective recovery of lithium from spent $LiMn_2O_4$ cathode materials.

Received 1st September 2025,
Accepted 20th November 2025

DOI: 10.1039/d5gc04585a

rsc.li/greenchem

Green foundation

1. This work advances green chemistry by developing a mild and selective oxidative delithiation route for $LiMn_2O_4$ that avoids high temperatures and strong acidic leaching, thereby reducing energy consumption and hazardous waste generation.
2. Using inexpensive and widely available sodium hypochlorite (NaClO) enables the direct production of λ-MnO_2 while selectively extracting lithium, with approximately 30% lower estimated carbon emissions and reduced reagent cost compared with persulfate-based processes.
3. Future research will emphasize safer handling of NaClO and addressing the risks of Cl_2 gas release to enhance process safety and scalability.

1. Introduction

Lithium-ion batteries (LIBs) were first successfully commercialized in 1991 by Sony using the $LiCoO_2$/C battery.[1] Since then, LIBs have been widely utilized in various areas, including portable devices (laptops, mobile phones, *etc.*) and handled devices, owing to their high energy densities, high coulombic efficiencies, and low self-discharge features.[1,2] Over the past several decades, growing concerns regarding climate change and fossil fuel security have led to a significant increase in the demand for electric vehicles (EVs).[2,3] This trend has directly contributed to a significant increase in the demand for LIBs. Among the various commercially available cathode materials, the spinel-type $LiMn_2O_4$ has garnered significant attention due to its high operating voltage, non-toxicity, low cost, and excellent thermal stability, making it useful for large-scale energy storage applications and EVs.[4–7] Therefore, the recycling of waste $LiMn_2O_4$ to obtain valuable raw materials, especially lithium, which has been listed as a critical raw

[a]*Graduate School of Creative Science and Engineering, Waseda University, Okubo 3-4-1, Shinju-ku, Tokyo 169-8555, Japan*
[b]*Faculty of Engineering, The University of Tokyo, Hongo 7-3-1, Bunkyo-ku, Tokyo 113-8656, Japan*
[c]*Research Institute for Science and Engineering, Waseda University, Okubo 3-4-1, Shinju-ku, Tokyo 169-8555, Japan*
[d]*Faculty of Science and Engineering, Waseda University, Okubo 3-4-1, Shinju-ku, Tokyo 169-8555, Japan. E-mail: tokoro@waseda.jp; Tel: +81-3-5286-3320*

material by many countries and regions, is of great importance. However, compared with other cathode materials, such as $LiCoO_2$, $LiNi_xCo_yMn_zO_2$, and $LiFePO_4$, studies on the recycling of $LiMn_2O_4$ are relatively limited.[6]

On the other hand, the rapid growth of lithium demand has not only driven the upsurge of selective lithium recovery from spent LIBs, but also led to the exploration of other available lithium resources. As reported, around 60% of the natural lithium reserves around the world exist in brines and sea water.[8] So far, many technologies, such as evaporation-precipitation,[9] solvent extraction,[10] membrane-based separation,[11,12] adsorption,[13,14] and electrochemical-based separation,[15,16] have been proposed to extract lithium from aqueous sources containing Na^+, K^+, Mg^{2+}, Ca^{2+}, *etc.*, especially from low-quality brines with high Mg^{2+}/Li^+ ratios.[17] Among them, lithium-selective ion sieves (LISs), typically derived from precursors containing Li^+ ions, are regarded as promising absorbents for separating lithium and obtaining high-purity products due to their excellent lithium selectivity.[8,17] In general, LISs can be divided into two categories according to their corresponding precursors: the lithium manganese oxides-type (LMO-type) and the lithium titanium oxides-type (LTO-type), with the former being more cost-effective than the latter due to the low cost of manganese compared to titanium.[8,14,17,18] As an important branch of LISs of the LMO-type, λ-MnO_2 is commonly prepared using spinel $LiMn_2O_4$ as precursor, in which the lithium sites are vacant and can accommodate Li^+ while excluding larger alkali such as Na^+, K^+ owing to size constraints and restricting divalent ions such as Mg^{2+} due to its high hydration enthalpy.[8,14,18–22] In order to improve the lithium uptake performance of λ-MnO_2-based absorbents, various strategies have been explored, including the development of λ-MnO_2 powders with diverse morphologies and increased surface areas,[23–25] and λ-MnO_2 composite materials with diatomaceous earth[14] and mesoporous polyacrylonitrile.[26] However, to date, the most common method for preparing λ-MnO_2 from $LiMn_2O_4$ still requires direct washing with inorganic acids such as HCl or HNO_3, with the associated cost of significant Mn loss (exceeding 20%).[13,14,20,27–29] Moreover, continuous acid treatment to extract lithium from the lithium-inserted λ-MnO_2-based absorbents would further induce Mn dissolution, severely impacting the performance and lifespan of λ-MnO_2 as a lithium ion-sieve.[14,30–32] Electrochemical delithiation provides a controllable and efficient route for lithium extraction from $LiMn_2O_4$[33] but typically requires conductive electrodes and complex reactor designs, making it less suitable for large-scale processing of powdery materials. Therefore, researchers proposed a hydrometallurgical strategy to selectively extract lithium from spinel $Li_xMn_2O_4$ ($0 < x \leq 1$) by using persulfate to inhibit Mn dissolution due to its strong oxidizing ability.[14,19,34–36] So far, various persulfates, such as $(NH_4)_2S_2O_8$, $K_2S_2O_8$, and $Na_2S_2O_8$, have been successively introduced. However, lithium extraction with persulfate typically requires a high operating temperature (above 80 °C), which undoubtedly increases the energy consumption. On the other hand, the hydrolysis of $S_2O_8^{2-}$ at higher temperatures generates a large amount of H^+, making the reaction solution highly acidic, posing a risk of partial Mn dissolution.[14,37] In addition, in the hydrometallurgical process, H_2O_2 predominantly acts as a reducing agent, facilitating the dissolution of $LiMn_2O_4$ through the reduction of Mn^{4+} to soluble Mn^{2+} species.[37] Therefore, developing a mild, efficient, and structurally preserving delithiation method can contribute to the sustainable utilization of lithium resources and solid wastes generated by spent LIBs in a circular economy context.

In this study, we propose a sodium hypochlorite (NaClO)-based delithiation approach that enables selective lithium extraction while maintaining the spinel framework integrity. As reported, NaClO works well across a wide range of pH at ambient temperature.[38–40] The Cl atom in NaClO exists as Cl^+, a strong electrophile that can accept two electrons and eventually reduce to Cl^-.[41] Furthermore, owing to its availability and lower price than other oxidants such as the above-mentioned persulfate, NaClO is widely used as an oxidant in daily life for sterilization and disinfection of drinking water.[42,43] More importantly, it is also effective at ambient temperature without requiring additional energy input, unlike persulfate, thereby offering a more controllable and energy-efficient approach for delithiation. Herein, we systematically investigated the performance of NaClO as an eluent for the selective recovery of lithium from spinel $LiMn_2O_4$, with the aim of simultaneously achieve the preparation of useful λ-MnO_2 under mild experimental conditions. The influencing factors of solution pH, NaClO dose, and solid-to-liquid ratio were studied on the lithium extraction process. In addition, the mechanisms involved during NaClO-driven delithiation using spinel $LiMn_2O_4$ as target were investigated. Meanwhile, comparative experiments were carried out using representative chemicals typically used in traditional λ-MnO_2 preparation (HCl and $Na_2S_2O_8$). In order to establish the capacity for lithium recovery, lithium uptake performances of delithiated $LiMn_2O_4$ sourced from NaClO, HCl, and $Na_2S_2O_8$ were assessed. In addition, a life cycle and tech-economic assessment was performed to provide a more comprehensive analysis of environmental footprints and energy consumption, reagent usage.

2. Experimental

2.1 Materials and reagents

A commercial $LiMn_2O_4$ cathode material was used in this study, which contains around 4.0% Li, and 70.2% Mn as determined by ICP-OES. Other chemical reagents, including sodium hypochlorite stock solution (NaClO with an initial available chlorine content approximately 12%), hydrochloric acid (HCl, 6 M and 1 M), sodium persulfate ($Na_2S_2O_8$), lithium chloride (LiCl) and lithium hydroxide monohydrate ($LiOH{\cdot}H_2O$), were of analytical grade and were purchased from FUJIFILM Wako Pure Chemical Corporation (Osaka, Japan). In addition, all solutions were prepared with ultrapure water (18.2 ΩM, 25 °C) sourced from a Millipore Milli-Q system (Bedford, MA, USA).

2.2 Experimental procedure

2.2.1 Leaching experiment. All experiments were conducted in a 100 mL glass beaker with a constant magnetic stirring rate to ensure uniform mixing. Firstly, the effect of solution pH on lithium extraction efficiency and Mn dissolution was studied. For this purpose, 1.0 g of $LiMn_2O_4$ cathode material were added into the glass beaker containing a predetermined volume of ultrapure water. Then, 4 mL of NaClO stock solution was added to the mixed solution, and the pH was adjusted to the target value using HCl (3, 4, 5, 6 and near-neutral (7–8)), marking the start of the experiment. The final total liquid volume was constant at 50 mL. A pH meter was used to monitor the solution's pH throughout the process, ensuring it remained within ±0.05 of the predetermined value. At the specific time intervals (15, 30, 60, 120, 240 and 360 min), a fixed volume of the solution was sampled and filtered through a 0.45 μm Teflon syringe filter for subsequent elemental analysis. In addition, other influencing factors such as initial NaClO dosage and solid–liquid ratio were also investigated following the same procedure. All the experiments were conducted at room temperature (25 °C).

2.2.2 Lithium uptake experiment. Lithium uptake experiments were conducted to evaluate the uptake properties of the obtained delithiated $LiMn_2O_4$ samples through different methods. The lithium-containing solutions were prepared using HCl, and LiCl and $LiOH{\cdot}H_2O$ as the lithium sources. 50 mg of delithiated $LiMn_2O_4$ were stirred in 50 mL of as-prepared lithium-containing solution with a constant lithium concentration of 15 mM for 24 hours to investigate the effect of solution pH on adsorption capacity. The solid-to-liquid ratio was fixed to 1 g L^{-1} for all experiments.

At the end of the experiment, solid–liquid separation was performed using vacuum filtration. The solid residue was thoroughly washed several times with ultrapure water and subsequently subjected to vacuum freeze-drying. The resulting solid was then used for further analysis.

2.3 Analytical method

2.3.1 Calculation method. The extraction efficiencies (E_i) of Li and Mn and the corresponding selectivity for lithium (SL) from the pristine $LiMn_2O_4$ were calculated using eqn (1) and (2).[44,45]

$$E_i = \frac{m_i \times V}{m \times w\%} \times 100\% \quad (1)$$

$$\mathrm{SL} = \frac{m_\mathrm{L}}{\sum m_i} \times 100\%, \quad (2)$$

where m_i is the concentration of element i in leachate, V is the volume of leachate, m is the mass used in each leaching experiment; w% is the mass fraction of metal in the pristine $LiMn_2O_4$. In addition, m_L is the concentration of lithium leached from pristine $LiMn_2O_4$.

Besides, the lithium uptake capacity of delithiated $LiMn_2O_4$ was calculated by eqn (3).[14]

$$Q_\mathrm{e} = \frac{(C_0 - C_\mathrm{e}) \times V}{m} \quad (3)$$

where Q_e (mg g^{-1}) refer to the normalized equilibrium; C_0 is the initial concentrations in solution; C_e is the equilibrium lithium concentration; V is the initial volume of solution, m (g) is mass of delithiated $LiMn_2O_4$ employed.

2.3.2 Material characterizations. Inductively coupled plasma optical emission spectrometry (ICP-OES; ICAP 6000 Series, Thermo Fisher Scientific, Waltham, USA) was used to determine the concentrations of Li and Mn in leachate. Crystal structural evaluation of the commercial $LiMn_2O_4$ upon delithiation were recorded by X-ray diffraction (XRD; Smartlab, Rigaku, Japan) with a Cu-Kα source operating at 40 kV and 15 mA. The step size was 0.01° and the scan rate was 3° min^{-1} in the 2θ range of 5°–80°. The morphological changes of the solid samples were analyzed by field-emission scanning electron microscopy (FESEM; JSM-6500F, JEOL, Japan). In addition, X-ray photoelectron spectroscopy (XPS; JPS-9010MX, JEOL, Japan) and nuclear magnetic resonance (NMR; JNM-ECA400, JEOL, Japan) analyses were conducted to investigate the changes in the chemical environment induced by lithium removal. In addition, the thermal behavior of pristine $LiMn_2O_4$ and delithiated $LiMn_2O_4$ samples were studied by thermogravimetry–differential thermal analysis (TG-DTA; TG8120, Rigaku, Japan) with a heating rate of 10 °C min^{-1} under a nitrogen gas flow, ranging from room temperature to 800 °C.

3 Results and discussion

3.1 Lithium extraction from spinel $LiMn_2O_4$ with NaClO

The variation of lithium extraction and Mn dissolution with solution pH at a fixed initial NaClO volume fraction were first investigated, and the corresponded results are depicted in Fig. 1(a) and (b), respectively. As shown in Fig. 1(a), the extraction efficiency of lithium increased significantly with the decrease of solution pH. In a circumneutral environment, approximately 41.7% of lithium was extracted into the aqueous solution. A significant increase in lithium extraction efficiency was observed with the decrease in solution pH. When the solution pH was reduced to 4, the lithium extraction efficiency significantly increased to about 99.3% after 6 hours of leaching, with no significant Mn dissolution occurring (Fig. 1(b)). Further decreasing the solution pH to 3 led to a lithium extraction efficiency comparable to the one achieved at pH = 4 but within a significantly shorter duration of just 2 hours. However, this also resulted in the Mn dissolution of 1.62%, as highlighted in Fig. 1(b). This means that excess HCl in the solution will cause structural Mn to dissolve.[46] Therefore, to achieve a high lithium leaching efficiency while preventing Mn loss, the solution pH should be carefully controlled at pH = 4. If not properly controlled, the Mn in the $LiMn_2O_4$ material will be dissolved into Mn^{2+} and subsequently will likely undergo a structural change due to the presence of strong oxidants such as HOCl, turning into other types of Mn oxides such as birnessite that precipitate on the surface. Such phenomenon was observed in the case of $Na_2S_2O_8$, as discussed in Section 3.3 of this study.

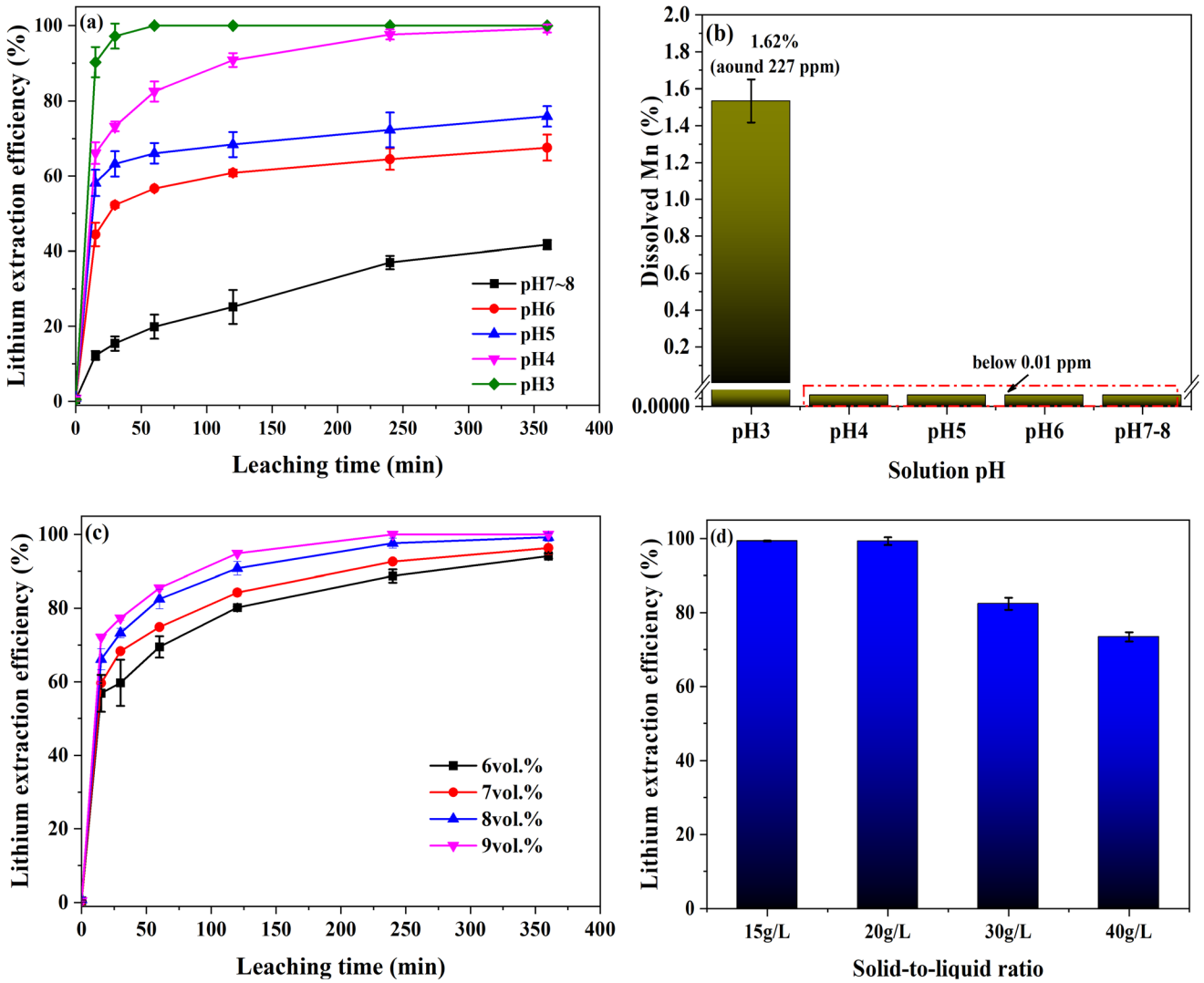

Fig. 1 The effect of different factors influencing lithium extraction efficiency: (a) different solution pHs and (b) the corresponding Mn dissolution (conditions: 20 g L^{-1} of solid-to-liquid ratio, 8% of initial NaClO volume fraction, 25 °C, 6 hours); (c) initial volume fraction of NaClO (conditions: 20 g L^{-1} of solid-to-liquid ratio, 25 °C, 6 hours), and (d) solid-to-liquid ratio (conditions: 8% of initial NaClO volume fraction, 25 °C, 6 hours).

Moreover, as illustrated in Fig. 1(c), at a constant solution pH of 4, the lithium extraction efficiencies all exceed 90.0% within the pre-determined initial NaClO dosage range of 6–9 vol%. The lithium extraction efficiency increases gradually and reaches 99.3% with the increasing initial volume fraction of NaClO equal to 8%. With a further increase in the initial volume fraction of NaClO to 9%, the extraction efficiency of lithium did not show a meaningful increase. For comparison, an experiment was performed at pH = 4 in the absence of NaClO. As presented in Fig. S1(a), the lithium extraction efficiency decreased to around 49.2%, accompanied by a Mn dissolution rate of 10.5%. This indicates the dual role of NaClO as suppressing Mn dissolution while facilitating lithium extraction as well. In addition to the above factors, the solid–liquid ratio is also an important factor affecting the lithium extraction process. As shown in Fig. 1(d), when the solid-to-liquid ratio is increased to 30 g L^{-1}, the lithium leaching efficiency decreases to 82.4% due to the rapid consumption of NaClO, which leads to a decrease in the oxidation capacity of the solution. Moreover, the reduced contact opportunities between solid particles and the reaction solution caused by the higher solid-to-liquid ratio will also have a significant negative impact on the lithium extraction efficiency.[44]

Based on the observations above, the following experimental conditions were selected for subsequent experiments to explore the delithiation mechanisms involved when using NaClO as an oxidant: a solid-to-liquid ratio of 20 g L^{-1}, an initial NaClO volume fraction of 8%, a solution pH of 4, a leaching temperature of 25 °C, and a reaction time of 6 hours. Theoretical calculations (based on available chlorine, which refers to chlorine equivalent) indicate that the residual oxidant concentration in the solution is approximately 0.64%,

suggesting that more than half of the NaClO remains in the leachate. As shown in Fig. S2, under the selected experimental condition, the obtained delithiated $LiMn_2O_4$ exhibits a reddish-brown color that is significantly different from the black pristine $LiMn_2O_4$.

3.2 Mechanistic elucidation of NaClO-driven lithium extraction from $LiMn_2O_4$

3.2.1 Actions of NaClO in the lithium extraction process. To gain a better understanding of the species present in aqueous solution as a function of solution pH and redox potential, Pourbaix plots were created by SPANA (formerly MEDUSA) software.[47] Fig. 2(a), (b) and Fig. S3 shows the E_h-pH diagrams of Mn–H_2O, Li–H_2O, and Cl–H_2O, respectively. The E_h-pH diagram in Fig. 2(a) reveals that Mn^{3+} can be oxidized to Mn^{4+} over a broad pH range of NaClO-containing solutions. Simultaneously, lithium is stable in the aqueous solution as Li^+ ions until pH > 13.5 (Fig. 2(b)). From this perspective, Li$[Mn^{3+}Mn^{4+}]O_4$ can be transformed into $[Mn^{4+}]O_2$ under near-neutral conditions (pH = 7–8), possibly resulting in lithium being simultaneously released into the surrounding aqueous media to maintain the electrical neutrality of the delithiated particles.[34,48,49] However, the fact is that only 41.7% of lithium was extracted, as shown in Fig. 1(a). This could occur because lithium ions are bound rather strongly to the spinel $LiMn_2O_4$ structure, as it has been reported that lithium ions are constrained within the tetrahedral cages with a deep site energy, endowing $LiMn_2O_4$-based LIBs with higher operating voltage (above 4 V).[5,50,51] Another possible reason is the increased migration path length, which requires lithium ions in the bulk phase to overcome a higher energy barrier compared to those on the surface or subsurface regions for extraction. In chemical oxidative lithium extraction, this is analogous to the oxidizing power of the reaction solution, which acts as the driving force for lithium extraction.[48,49] Therefore, the oxidizing power provided by the chosen oxidant to overcome the energy barrier plays a crucial role in determining the efficiency of lithium extraction.

The chlorine speciation of NaClO in aqueous solution is strongly pH-dependent.[39,41,42] As shown in eqn (4)–(6) and Fig. S3, the main chlorine species, Cl_2, HOCl, and OCl^-, exist in equilibrium depending on the solution pH. Around neutral pH, HOCl and OCl^- are the dominant species. As the pH decreases, HOCl becomes predominant, and at even lower pH values (below 3.33), Cl_2 starts to form. Because HOCl has a higher redox potential ($E°$(HOCl/Cl^-) = +1.49 V) than both OCl^- and Cl_2, the oxidation ability of NaClO solution increases as the proportion of HOCl rises.[41] Moderate acidification (pH ≈ 4) therefore enhances lithium extraction from $LiMn_2O_4$, as the stronger oxidative power of HOCl facilitates lithium removal from the spinel lattice. However, excessive acidification produces Cl_2 gas, which is toxic and corrosive,[39,41] and also promotes Mn dissolution through H^+ attack. Hence, maintaining the solution near pH = 4 provides an optimal balance between oxidation strength and structural stability of $LiMn_2O_4$. In this case, HOCl serves as the main oxidizing species, promoting the extraction of lithium from the solid phase into solution while minimizing Cl_2 evolution. In addition, reducing the solid-to-liquid ratio to 15 g L^{-1}, while maintaining a lithium extraction efficiency comparable to that at 20 g L^{-1} (as shown in Fig. S1(b), with an efficiency of about 98.7%), extends the operable pH range to 4.5, thereby further minimizing the likelihood of Cl_2 evolution. Furthermore, NaClO can be safely handled through closed circulation and storage systems to minimize volatilization and operator exposure. Continuous pH monitoring and automated alkali dosing can also be employed to maintain the solution within a mildly acidic range (around pH range of between 4 to 4.5), effectively suppressing Cl_2 generation. In addition, pretreatment processes such as particle size reduction (*e.g.*, ball

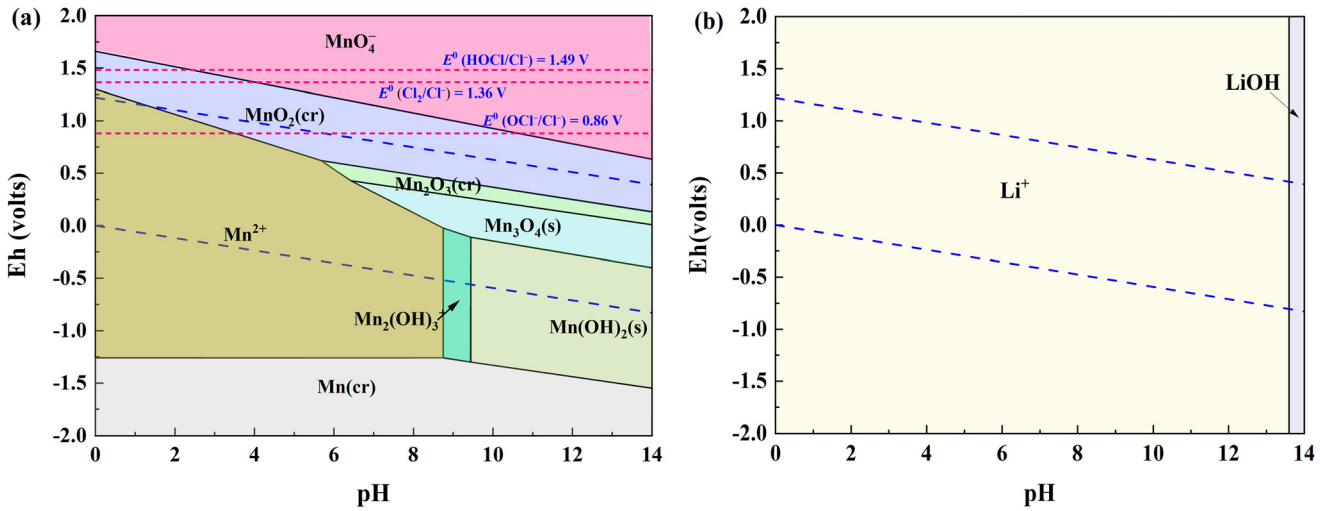

Fig. 2 E_h-pH diagram for the (a) Mn–H_2O system and (b) Li–H_2O system (T = 298.15 K, the molar concentration of Mn and Li was fixed at 1 × 10^{-3} mol L^{-1} and 0.1 mol L^{-1}, respectively).

milling) may further broaden the operating pH window and enhance process stability.

$$NaClO \rightarrow Na^+ + OCl^- \quad (E^\circ(ClO^-/Cl^-) = +0.89\ V\ vs.\ SHE) \tag{4}$$

$$OCl^- + H_2O \rightarrow HOCl + OH^- \quad (E^\circ(HOCl/Cl^-) = +1.49\,V\,vs.\,SHE, pK_a = 7.60) \tag{5}$$

$$HOCl + H^+ + Cl^- \rightarrow Cl_2 + H_2O \quad (E^\circ(Cl_2/Cl^-) = +1.36\,V\,vs.\,SHE, pK_a = 3.33) \tag{6}$$

3.2.2 Characterizations of delithiated $LiMn_2O_4$ with NaClO. The changes in morphology due to the NaClO-driven delithiation at pH = 4 were studied by FE-SEM. Fig. 3 displays the micrographs of pristine $LiMn_2O_4$ and NaClO-derived delithiated $LiMn_2O_4$ sample at the selected experimental conditions. The pristine $LiMn_2O_4$ particles exhibit smooth surfaces with a well-defined facet (Fig. 3(a)). As shown in Fig. 3(b), the delithiated particles largely retained their original shape and smooth surface. However, a few irregularly shaped particles with wrinkled surfaces were observed (Fig. 3(b-2)), indicating the occurrence of localized surface damage induced by H^+ attack. This suggests that a small amount of Mn was initially dissolved in the weakly acidic environment but was rapidly oxidized and subsequently precipitated as a solid.

To investigate the structural changes during lithium extraction, a representation approach for lithium content within the host structure was employed. This approach consists in representing the crystal structure with the simplified formula $Li_xMn_2O_4$, where the subscript x is a calculated value from the ICP-OES results, indicating the average lithium content remaining in delithiated material after leaching, and can take values in the range $0 < x < 1$.[52–54] Therefore, samples with varying lithium contents were prepared under the selected experimental conditions (initial NaClO volume fraction of 8%, 20 g L^{-1} of solid-to-liquid ratio, pH = 4, 6 hours, a leaching temperature of 25 °C). The XRD patterns of these samples were subsequently collected and are shown in Fig. 4(a). Moreover, the variation of cell parameter a in $Li_xMn_2O_4$ was calculated derived from the (400) peak, as its behavior closely correlates with the lithium extraction process,[54] the corresponding results are summarized in Table S1. As clearly shown in Fig. 4(a), the XRD pattern changes of $LiMn_2O_4$ during the delithiation process proceeds through two stages.[52,53,55] In the initial stage of lithium extraction ($x \leq 0.43$ in $Li_xMn_2O_4$), corresponding to a single-phase region, the diffraction peaks shifted gradually toward higher 2θ angles. This shift is attributed to the isotropic contraction of the unit cell, resulting from the topotactic extraction of lithium from the $LiMn_2O_4$ crystal structure. During this stage, the lattice parameter a decreased from 8.25 Å in pristine $LiMn_2O_4$ to 8.15 Å and stabilizes at this value in the subsequent delithiation process, as shown in

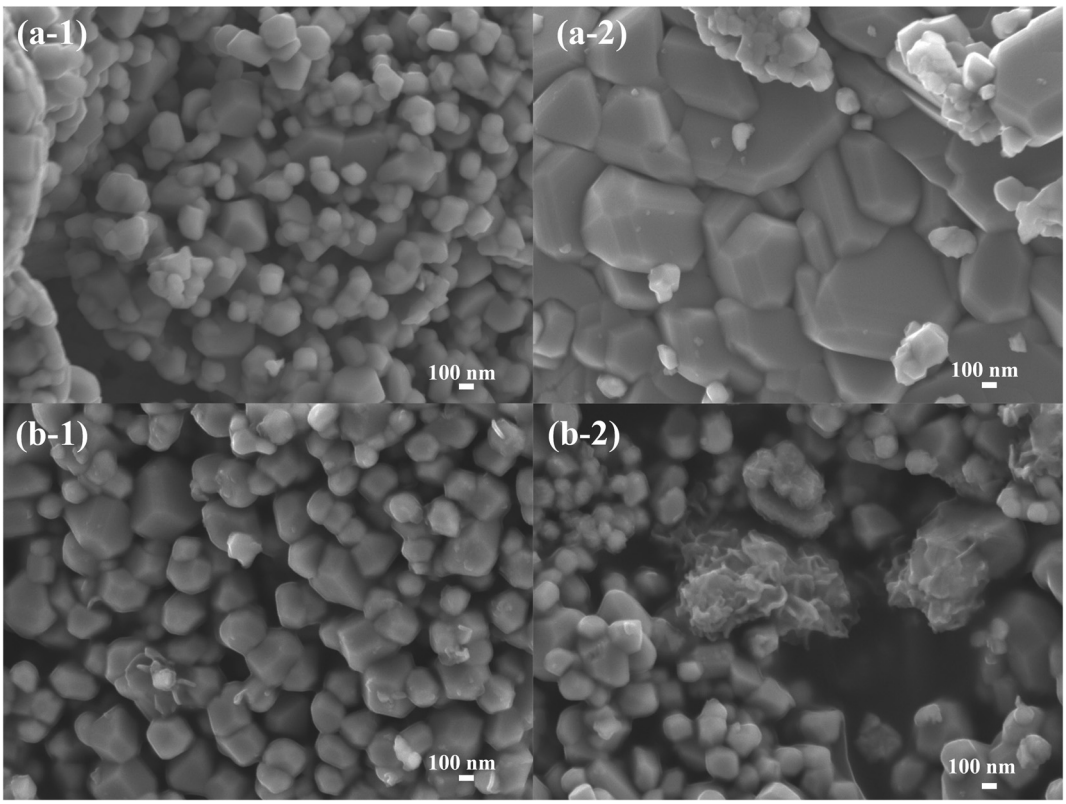

Fig. 3 Surface morphology changes of (a) pristine $LiMn_2O_4$ and (b) NaClO-derived delithiated $LiMn_2O_4$ sample at the selected leaching conditions.

Table S1. In contrast to the first stage, the second stage corresponds to the coexistence of two phases. At $x = 0.3$ in $Li_xMn_2O_4$, the diffraction peaks were clearly split, as shown in the enlarged 2θ ranges of 17.5–19.5° and 43–46° in Fig. 4(a). After that, as the lithium content in $Li_xMn_2O_4$ further decreases, the intensities of the newly split peaks progressively increase, while the original shifted peaks diminish. Eventually, the diffraction pattern evolved into a single-phase structure with a lattice parameter $a' = 8.045$ Å, consistent with previous reports on lithium extracted electrochemically from $LiMn_2O_4$.[52,56] The final phase was indexed to spinel λ-MnO_2 (PDF card no: 00-044-0992), whose structure retains lithium vacancies that only allow lithium and hydrogen ions to enter.

In addition, ^{7}Li MAS NMR spectroscopy and XPS were performed to get an insight on the local environment changes in the $LiMn_2O_4$ structure as a function of delithiation, as presented in Fig. 4(b) and (c). In the cases of pristine $LiMn_2O_4$ and $Li_{0.43}Mn_2O_4$, their ^{7}Li MAS NMR spectra exhibit prominent spinning sideband manifolds. For the pristine $LiMn_2O_4$ sample, its spectrum is dominated by a major resonance at around 520 ppm, corresponding to lithium ions occupying the tetrahedral sites, with an average Mn oxidation state of +3.5.[54,57,58] As lithium is extracted, the ^{7}Li MAS NMR spectrum of $Li_{0.43}Mn_2O_4$ shifts toward a more positive value, as shown in Fig. 4(b), indicating an increase in the proportion of Mn^{4+} in the delithiated particles.[54] Meanwhile, the ^{7}Li MAS NMR

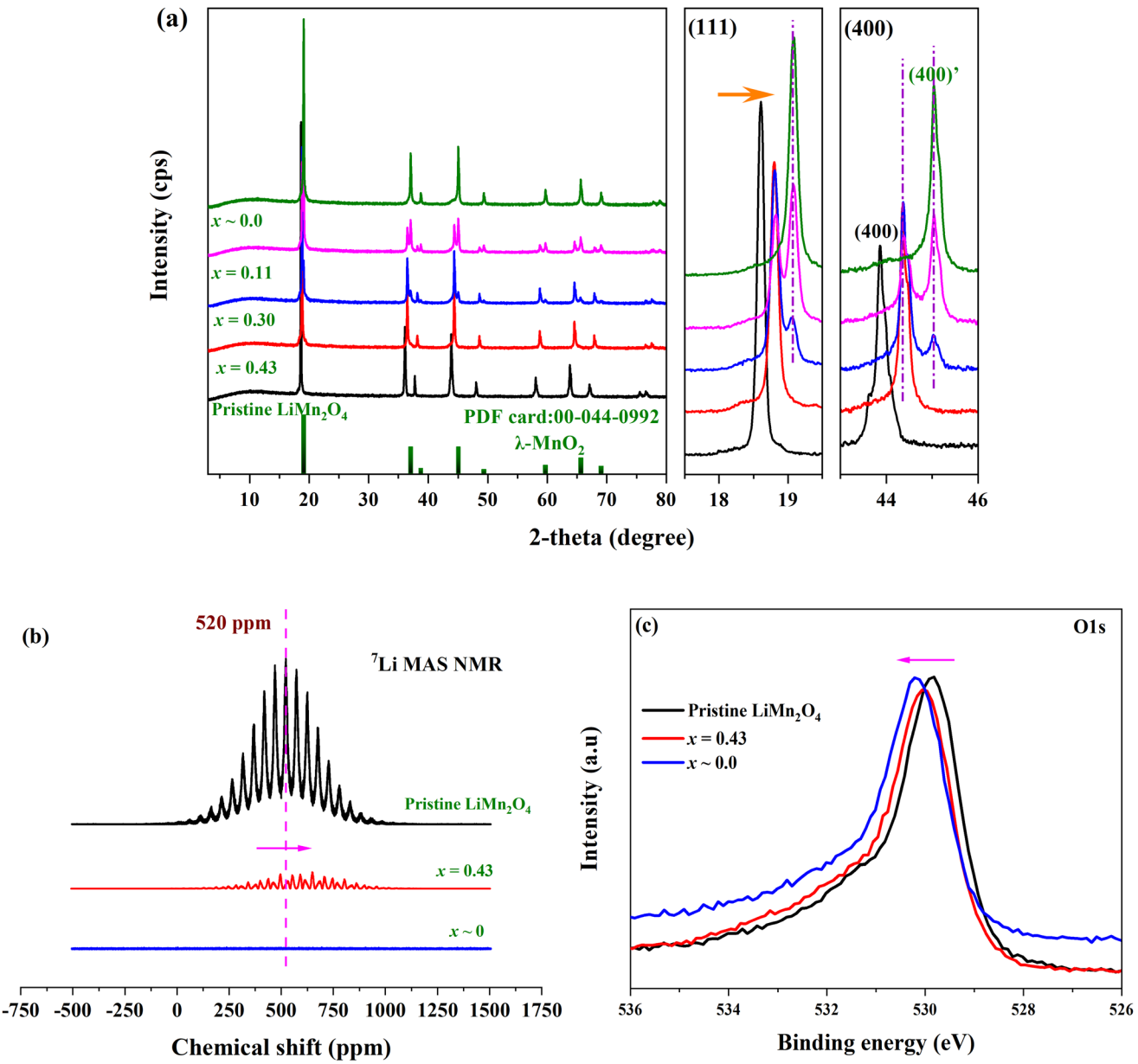

Fig. 4 (a) X-ray diffraction patterns, (b) ^{7}Li MAS NMR spectra, and (c) high-resolution O 1s XPS spectra collected from $Li_xMn_2O_4$ with different lithium contents.

spectra intensity gradually weakened with decreasing lithium content and finally became undetectable after 6 hours of leaching. This further evidenced by the evolution of high-resolution O 1s XPS spectra. As illustrated in Fig. 4(c), the main peak of O 1s XPS spectra, initially located at approximately 529.8 eV, progressively shifts to higher binding energies as lithium extraction proceeds. This shift reflects changes in the chemical environment of oxygen, attributed to the oxidation of Mn^{3+} caused by lithium extraction.[37] The evolution of average Mn oxidation state during NaClO-driven delithiation process was thoroughly investigated using Mn 3p and Mn 3s XPS spectra to get deeper understanding, and the results are shown in Fig. 5. In addition, the average oxidation state (AOS) of Mn was calculated using eqn (7).[59–61]

$$\mathrm{AOS} = 8.956 - 1.126 \times \Delta E_s \ (\mathrm{eV}) \quad (7)$$

where, ΔE_s refers to the magnitude of the Mn 3s peak splitting, and the corresponded results are summarized in Table 1. As depicted in Fig. 5(a), the high-resolution Mn 3p XPS spectra can be deconvoluted into two components: Mn(IV) (~50.4 eV) and Mn(III) (~48.8 eV).[62] Upon delithiation, the Mn^{4+} content in the delithiated samples gradually increases, while Mn^{3+} correspondingly decreases. This is evidenced by the multiple splitting of Mn 3s as shown in Fig. 5(b) and Table 1, where the values of ΔE_s decreases, indicating an increase in the AOS of Mn in the delithiated $LiMn_2O_4$ samples, consistent with the results revealed by both ^{7}Li MAS NMR and O 1s XPS analyses. In addition, it is noteworthy that a high-resolution Li 1s XPS signal centered at around 54 eV was observed for the pristine $LiMn_2O_4$ sample, which is close to the Mn 3p peak.[62,63] As the lithium content decreases, the intensity of the high-resolution XPS Li 1s signal gradually weakens and ultimately disappears. This indicates the progressive depletion of lithium in the surface region of delithiated particles, aligning with the changes in the average oxidation state of Mn and the structural changes detected through XRD.

Table 1 Changes in the AOS of Mn upon delithiation

Samples	ΔE_s	AOS
Pristine $LiMn_2O_4$	4.8507	3.494
$x = 0.43$	4.6018	3.774
$x = 0.30$	4.5379	3.846
$x = 0.11$	4.4705	3.922
$x \sim 0.0$	4.4214	3.978

Fig. 6(a) shows the TG-DTA curves for pristine $LiMn_2O_4$ and NaClO-derived delithiated $LiMn_2O_4$ after 6 hours of leaching under the selected leaching condition. The pristine $LiMn_2O_4$ almost remains stable until to around 600 °C. In contrast, as shown in the TG curve of NaClO-derived delithiated $LiMn_2O_4$ sample, the weight loss can be divided into two stages occurring in the low temperature region (below 300 °C) and high

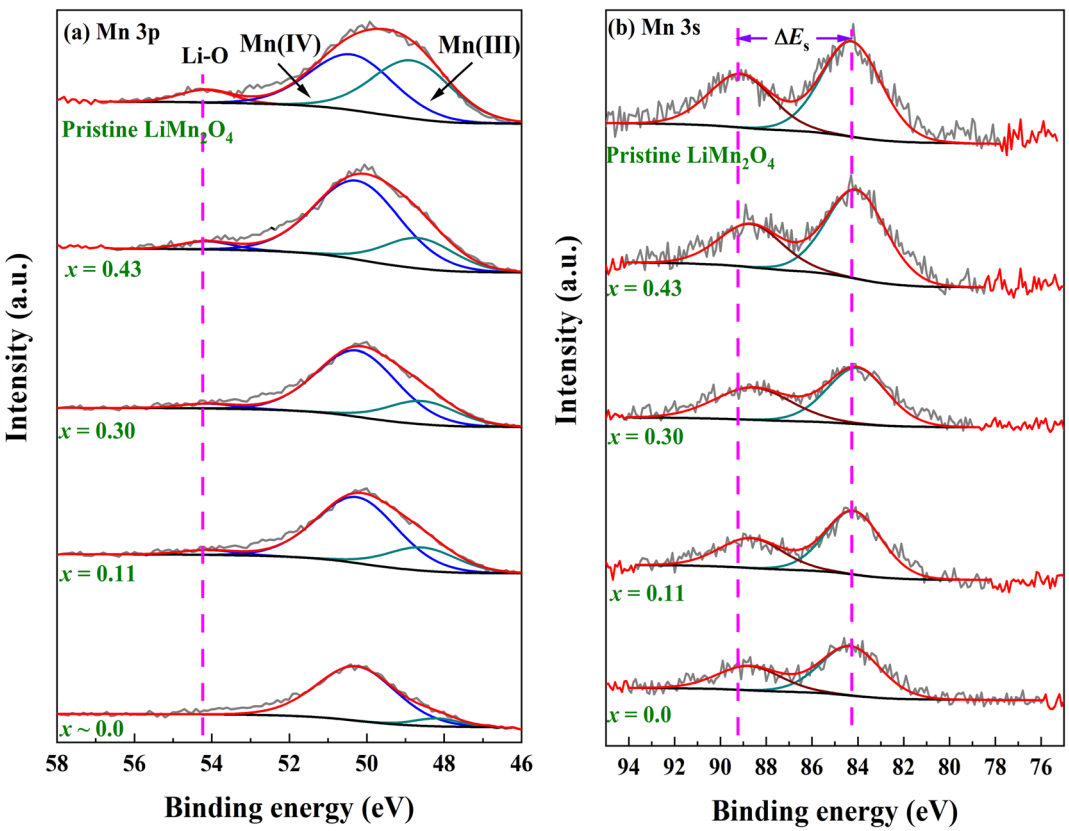

Fig. 5 High-resolution XPS spectra of (a) Mn 3p and (b) Mn 3s collected from $Li_xMn_2O_4$ with different lithium contents.

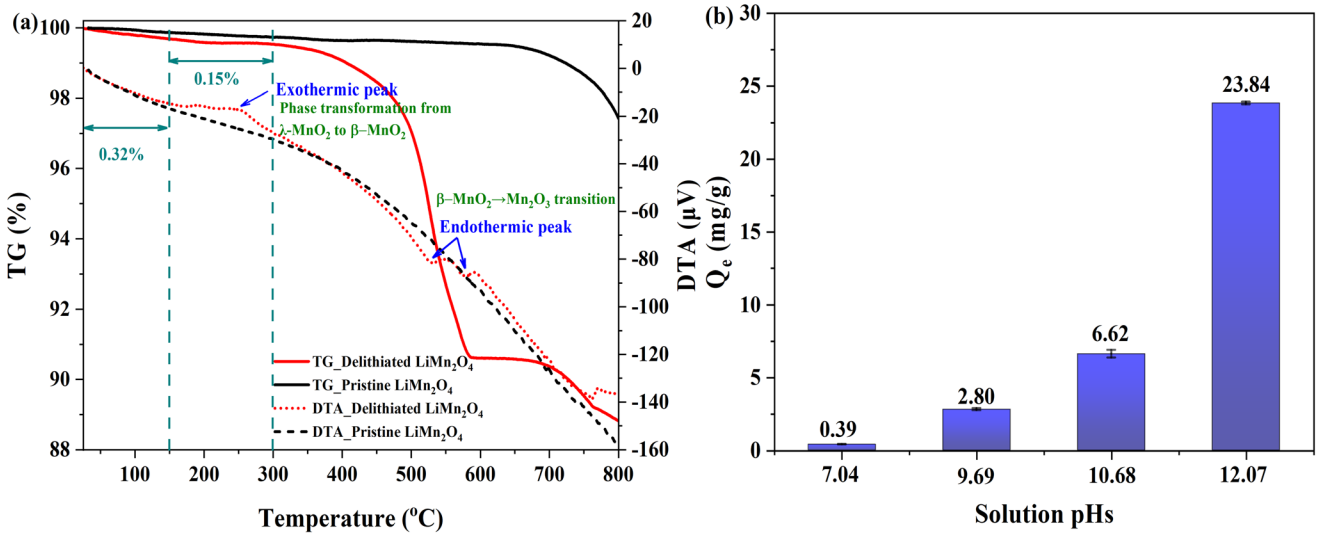

Fig. 6 (a) TG-DTA curves of the pristine $LiMn_2O_4$ (black line) and NaClO-derived delithiated $LiMn_2O_4$ (red line); (b) the influence of pH on the Li^+ adsorption behaviors of NaClO-derived $LiMn_2O_4$ (experimental conditions: 1 g L^{-1} of solid-to-liquid ratio, 15 mM of Li^+, 25 °C, 24 hours).

temperature region (300–600 °C). In the low temperature region, a slight weight loss started from room temperature to below 150 °C, possibly owing to the evaporation of physically absorbed water on the surface of delithiated particles. Moreover, a broad exothermic peak was observed at approximately 250 °C, which corresponds to the phase transformation from spinel λ-MnO_2 to β-MnO_2 at higher temperatures.[20,22] When increasing the treatment temperature above 350 °C, a remarkable weight loss was observed. The endothermic peaks observed in the 500–600 °C range are thought to result from the transition of β-MnO_2 to Mn_2O_3 by the reduction of Mn^{4+} in the N_2 atmosphere.[20,22]

Importantly, the weight loss (approximately 0.15%) observed in the TG curve of NaClO-derived delithiated $LiMn_2O_4$ sample at 150–300 °C can be ascribed to the presence of lattice protons in the delithiated sample.[37,64] In order to further verify whether H^+ exists in the NaClO-derived delithiated $LiMn_2O_4$ particles, lithium uptake experiments were performed at different solution pHs. Earlier studies have suggested that lithium ions can be inserted into the lithium vacancies formed by redox reaction only under alkaline conditions, whereas lithium uptake in OH^--free solutions can occur solely through a H^+/Li^+ ion-exchange reaction.[21] As depicted in Fig. 6(b), the NaClO-derived delithiated $LiMn_2O_4$ sample demonstrated a relatively low lithium uptake capacity of only 0.39 mg g^{-1} in a pure LiCl solution. In contrast, the lithium uptake capacity of the NaClO-derived delithiated $LiMn_2O_4$ sample significantly increased when the solution pH was raised, ultimately reaching 23.84 mg g^{-1} in a pure LiOH solution, which is equivalent to around 60.02% of the theoretical maximum lithium adsorption capacity of the NaClO-derived delithiated $LiMn_2O_4$. There are many factors that limit the further entry of lithium into the de-lithiated $LiMn_2O_4$, such as the initial pH value of the solution and the reaction temperature, *etc*. For example, increasing the reaction temperature of the solution can effectively improve the adsorption performance of delithiated $LiMn_2O_4$.[14]

Combined with the solid analysis presented in Fig. S4 and S5 in the SI, it is postulated that NaClO-driven lithium extraction from $LiMn_2O_4$ at pH = 4 involves two reactions: redox reaction and Li^+/H^+ ion-exchange reaction, as described in eqn (8) and (9).

Redox pathway (major):

$$Li[Mn^{III}Mn^{IV}]O_4 + y/2HClO \rightarrow Li_{1-y}[Mn^{IV}_{1+y}Mn^{III}_{1-y}]O_4 + yLi^+ + y/2OH^- + y/2Cl^- \quad (8)$$

Ion-exchange pathway (minor):

$$Li[Mn^{III}Mn^{IV}]O_4 + zH^+ \rightarrow Li_{1-z}H_z[Mn^{III}Mn^{IV}]O_4 + zLi^+ \quad (9)$$

where □ refers the lithium vacancies after lithium removal; y, z is the extracted lithium amount from pristine $LiMn_2O_4$ through redox reaction and ion-exchange reaction, respectively. Under the action of NaClO at pH = 4, the redox mechanism associated with the oxidation of Mn^{3+} to Mn^{4+} dominates lithium extraction process, converting $LiMn_2O_4$ to λ-MnO_2. In addition, the ion-exchange mechanism, where Li^+ ions are replaced by H^+ from the acidic solution, also occurs but makes a minor contribution to the overall lithium extraction. Notably, the ion exchange reaction does not lead to changes in Mn oxidation state, which is consistent with the statistical results presented in Table 1.

3.3 Comparison with other methods for preparing spinel λ-MnO_2

As mentioned above, there are two primary methods for preparing λ-MnO_2 (delithiated $LiMn_2O_4$) using spinel $LiMn_2O_4$ as

a precursor: acid treatment and oxidant treatment, with the latter typically involving persulfate use, as listed in Table S2. Clearly, acid treatment (*e.g.*, using HCl, HNO_3, or H_2SO_4) can achieve efficient lithium extraction under strongly acidic conditions (typically at pH ≤ 1), but it results in more than 20% of Mn loss. Oxidant-based methods using persulfates such as $Na_2S_2O_8$ or $(NH_4)_2S_2O_8$ generally require elevated temperatures (typically 80–90 °C). In contrast, the NaClO-based oxidation route overcomes these limitations, enabling efficient lithium extraction without Mn loss under ambient temperature and mildly acidic conditions. To further emphasize the advantages of the method proposed in this study, lithium extraction experiments were conducted using representative reaction conditions commonly used in previous studies; that is, 0.5 M HCl and 0.2 M $Na_2S_2O_8$, respectively. The other experimental conditions were the same as our study (*i.e.*, a solid-to-liquid ratio of 20 g L^{-1} and a reaction duration of 6 hours). Moreover, experiments of lithium extraction with $Na_2S_2O_8$ were performed at different reaction temperatures (room temperature (T = 25 °C), T = 45 °C and $T \geq 80$ °C).

As demonstrated in Fig. 7(a), almost all lithium can be extracted using 0.5 M HCl at T = 25 °C; however, this was accompanied by a significant Mn loss from the $LiMn_2O_4$ structure equal to 23.8%. The molar ratio of Li^+ to Mn^{2+} in the leachate was calculated to be approximately 2 : 1, which is in good agreement with the observations at pH = 4 in the absence of NaClO. This indicates that lithium extraction in acidic solutions without oxidants mainly occurs through the disproportionation reaction of Mn^{3+} to Mn^{2+} and Mn^{4+}. The Mn^{2+} enters the acidic solution, while Mn^{4+} remains in the solid framework in the form of λ-MnO_2, as evidenced by the XRD results shown in Fig. S6. The corresponding reaction can be described as eqn (10).[20] Correspondingly, as shown in Fig. 7(b)-(A-1) and (A-2), HCl-treated $LiMn_2O_4$ particles lost their original smooth surface and well-defined facets, instead resulting in particles filled with pores and cracks due to the partial dissolution of

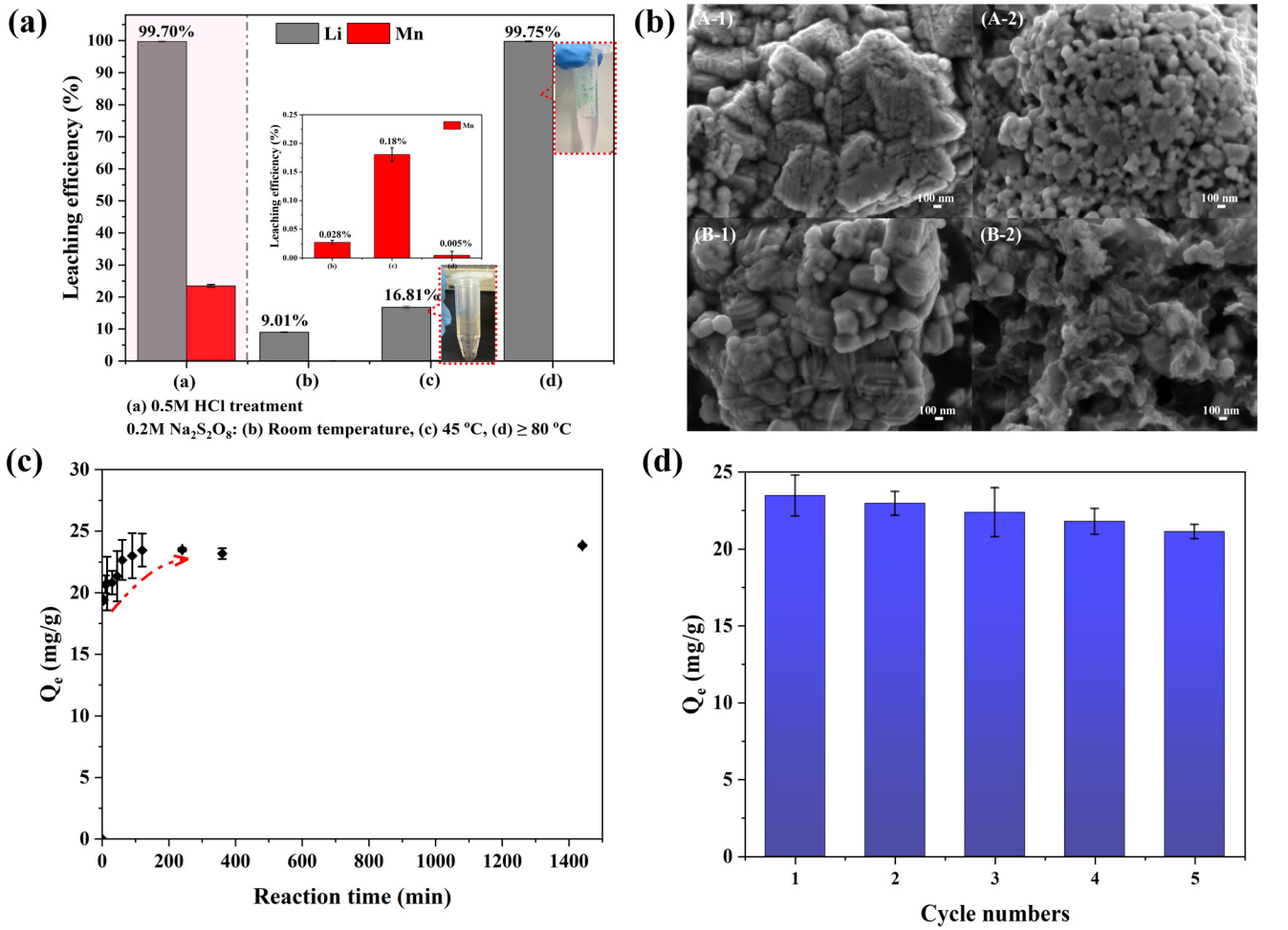

Fig. 7 (a) Leaching efficiencies of Li and Mn from $LiMn_2O_4$ using HCl and $Na_2S_2O_8$; (b) surface morphology changes of the obtained delithiated $LiMn_2O_4$ samples by (A) 0.5 M HCl and (B) 0.2 M $Na_2S_2O_8$ at $T \geq 80$ °C; (c) time-dependent lithium uptake process using NaClO-derived λ-MnO_2 as sample (experimental conditions: 1 g L^{-1} of solid-to-liquid ratio, 15 mM of Li^+, 25 °C, 24 hours, initial solution pH = 12.07); (d) cyclic performance of the NaClO-derived λ-MnO_2 (experimental conditions: 1 g L^{-1} of solid-to-liquid ratio, 15 mM of Li^+, 25 °C, 2 hours, initial solution pH = 12.07).

Mn from parent $LiMn_2O_4$, which eventually fractured into smaller particles.

$$2LiMn_2O_4 + 4H^+ \rightarrow 2Li^+ + Mn^{2+} + 2H_2O + 3\lambda\text{-}MnO_2 \quad (10)$$

In contrast to NaClO and HCl, $Na_2S_2O_8$-based oxidative delithiation shows poor activity at low temperatures. As shown in Fig. 7(a), only 9.12% of lithium was removed from $LiMn_2O_4$ at room temperature. Increasing the temperature to 45 °C improved Li extraction to 16.5%, but also raised the Mn dissolution rate from 0.03% to 0.17%. The leachate turned black after standing overnight, indicating the presence and subsequent oxidation of Mn^{2+} species. When the temperature exceeded 80 °C, lithium extraction reached a level comparable to 0.5 M HCl treatment, while the leachate became highly acidic (pH ≈ 1.07) with a pale pink hue, suggesting trace formation of MnO_4^- (<0.05 ppm). These observations highlight the strong temperature dependence of $Na_2S_2O_8$ oxidation. As temperature increases, the hydrolysis of $S_2O_8^{2-}$ accelerates, generating $^{\bullet}OH$ and $SO_4^{\bullet-}$ radicals (eqn (11) and (12))[37,44] that enhance lithium extraction. However, $SO_4^{\bullet-}$ also promotes H^+ and H_2O_2 formation (eqn (13) and (14)), which leads to acid-driven Mn dissolution.[14,30,37] At temperatures above 80 °C, H_2O_2 decomposes rapidly (eqn (15)), effectively suppressing Mn loss,[14,37] as confirmed by the ICP–OES data in Fig. 7(a).

$$S_2O_8^{2-} \rightarrow 2SO_4^{\bullet-} \quad (11)$$

$$SO_4^{\bullet-} + H_2O \rightarrow {}^{\bullet}OH + HSO_4^- \quad (12)$$

$$SO_4^{\bullet-} + 2H_2O \rightarrow SO_4^{2-} + 2H^+ + H_2O_2 \quad (13)$$

$$2LiMn_2O_4 + 10H^+ + H_2O_2 \rightarrow 4Mn^{2+} + 2Li^+ + 6H_2O + 2O_2 \quad (14)$$

$$2H_2O_2 \rightarrow 2H_2O + O_2 \quad (15)$$

Consistent with the above observations, the XRD pattern of the $Na_2S_2O_8$-treated samples shows (Fig. S6), in addition to the characteristic reflections of λ-MnO_2, an additional diffraction peak at around $2\theta \approx 12°$, indicating the formation of a new phase. Similar features have been reported in previous studies[19,30,37] and is identified here as $Na_{0.364}MnO_2(H_2O)_{0.54}$ (PDF 01-072-6745), a birnessite-type compound. The corresponding morphological evolution, shown in Fig. 7(b)-(B-1) and (B-2), further corroborates this phase transformation. The dissolved Mn^{2+} species are rapidly re-oxidized by strong oxidizing radicals ($SO_4^{\bullet-}$ and $^{\bullet}OH$) to form birnessite-like Mn oxides.[44,65,66] Such secondary reactions alter the surface chemistry of the resulting λ-MnO_2 and ultimately impair its lithium re-insertion capability.[67]

As shown in Fig. S7, when compared with the λ-MnO_2 samples sourced from NaClO and HCl, $Na_2S_2O_8$-derived λ-MnO_2 sample exhibited a reduced lithium uptake of 20.55 mg g^{-1} in pure LiOH solution. This decrease may be due to the presence of a birnessite-like phase on the surface of the resulting λ-MnO_2 particles would hinder direct contact between the λ-MnO_2 particles and the reaction solution, limiting lithium uptake. In addition, the cyclic performance of the NaClO-derived λ-MnO_2 was evaluated through repeated adsorption–desorption tests, during which the variations in lithium uptake capacity and Mn dissolution were systematically monitored in a pure LiOH solution. Prior to these tests, a 24-hour time-dependent lithium uptake experiment was conducted to determine the adsorption equilibrium point, as shown in Fig. 7(c). The results indicate that equilibrium was achieved within 2 hours; therefore, the adsorption duration in subsequent cycling tests was fixed at 2 hours. As presented in Fig. 7(d), the lithium uptake capacity remained as high as 89.9%, decreasing only slightly from 23.46 to 21.11 mg g^{-1} after five cycles. Meanwhile, negligible Mn dissolution was detected. The minor capacity loss can be attributed to lattice contraction and expansion during repeated adsorption–desorption processes, which generate mechanical stress and gradually cause structural deformation or partial collapse of the three-dimensional lithium channels.

3.4 Life cycle and techno-economic assessments

A simplified flowchart of the three methods is presented in Fig. S8. To assess the environmental sustainability of the proposed method in this study, a comparative life cycle assessment (LCA) was conducted against the HCl- and $Na_2S_2O_8$-based (≥80 °C) processes. For comparison, 1 kg of commercial $LiMn_2O_4$ was selected as the functional unit, and the corresponding material flows for the three processing routes are summarized in Table S3. The LCA was conducted using openLCA in combination with the Ecoinvent 3.10 database, and the resulting environmental indicators are presented in Table S4. In parallel, a techno-economic evaluation was performed to assess and compare the total costs of the three processing routes, thereby providing insight into their respective economic feasibility, as shown in Table S5. Furthermore, these three methods were comparatively analyzed in terms of energy and water consumption, λ-MnO_2 yield, and downstream treatment with the goal of lithium recovery, enabling a holistic assessment of both environmental and economic performance.

Fig. 8(a) presents a visual comparison of the overall environmental impacts of the HCl-, $Na_2S_2O_8$-, and NaClO-based delithiation processes. The cumulative impacts related to ozone layer depletion and eutrophication were negligible across all processing routes, rendering a reliable comparison impractical. Therefore, these two categories were excluded from further analysis. Overall, the $Na_2S_2O_8$-based process exhibits the highest environmental burdens among the three routes. In detail, compared with the traditional acid treatment, the NaClO-based process demonstrates markedly lower impacts in human toxicity and freshwater aquatic ecotoxicity. As both are oxidative delithiation, the NaClO-based process is significantly superior to $Na_2S_2O_8$ in terms of key indicators shown in Fig. 8(a). In addition, Fig. 8(b) and Fig. S9(a)–(c) present a comprehensive comparison from a techno-economic perspective. Specifically, the total processing cost of the proposed NaClO-based route is slightly lower than that of the HCl-based process, achieving a cost reduction of $2.07 per kg of feedstock, and accounts for only 45.8% of the cost of the

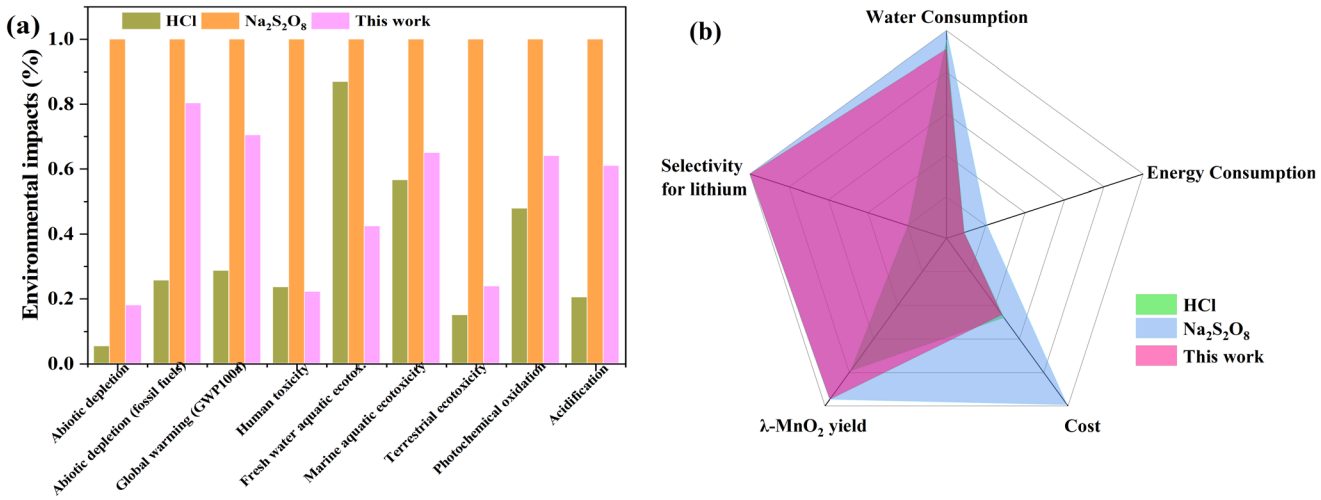

Fig. 8 (a) Environmental impact assessment and (b) techno-economic analysis of three processing methods.

$Na_2S_2O_8$-based route. In contrast, the traditional acid leaching method performs the poorest in terms of λ-MnO_2 yield (Fig. S9(b)). Even worse, its extensive dissolution of Mn leads to poor lithium selectivity (Fig. S9(c)). This necessitates an additional Mn precipitation–filtration step in the subsequent lithium recovery process, which inevitably causes lithium loss and reduces the purity of the recovered lithium product. Consequently, further purification steps are needed, increasing both energy and reagent consumption (*e.g.*, NaOH).

4 Conclusions

This study demonstrates that NaClO is an effective and sustainable oxidant for the selective extraction of lithium from spinel $LiMn_2O_4$ under mild conditions (room temperature, pH = 4). The extraction efficiency reached 99.3% within 6 hours without Mn loss, primarily driven by Mn^{3+} oxidation and H^+/Li^+ ion exchange. Unlike HCl or $Na_2S_2O_8$ treatments, the NaClO process causes negligible structural damage to $LiMn_2O_4$, owing to its weaker acidity and tunable oxidizing strength. From an environmental and techno-economic perspective, the NaClO-based oxidative delithiation route performs markedly better than that of $Na_2S_2O_8$ oxidation, while costing only about 45.8% as much. From a standalone process perspective, the NaClO-based route shows slightly higher impacts than the conventional acid leaching method in some environmental categories; however, it offers pronounced advantages during the subsequent treatment stages. For future scale-up, the proposed method in this study still faces several challenges due to rigid infrastructure and market immaturity, particularly in NaClO handling in bulk, pH control in continuous processes, risk of Cl_2 evolution. Lowering the solid-to-liquid ratio or introducing a pretreatment step, such as ball milling to reduce particle size, may help raise the solution pH to a higher level, thereby effectively suppressing Cl_2 formation and enhancing operational safety.

Author contributions

Yanhui Kong: data curation, formal analysis, writing – original draft, conceptualization, methodology, writing – review & editing. Yutaro Takaya: writing – review & editing. Mauricio Córdova-Udaeta: writing – review & editing. Chiharu Tokoro: supervision.

Conflicts of interest

The authors declare that they have no known competing financial interests or personal relationships that could have appeared to influence the work reported in this paper.

Data availability

All the data provided in this article are included within the figures and tables of this article and the supplementary information (SI). Supplementary information is available. See DOI: https://doi.org/10.1039/d5gc04585a.

Acknowledgements

We thank the Kagami Memorial Research Institute for Materials Science and Technology, and the Materials Characterization Central Laboratory, Waseda University for the solid analysis. Yanhui Kong gratefully acknowledges financial support of Ministry of Education, Culture, Sports, Science and Technology (MEXT), Japan.

References

1 T. Kim, W. Song, D. Son, L. K. Ono and Y. Qi, *J. Mater. Chem. A*, 2019, 7(7), 2942–2964.

2 J. B. Goodenough and K. S. Park, *J. Am. Chem. Soc.*, 2013, **135**(4), 1167–1176.
3 G. Harper, P. Slater, R. Sommerville, R. Stolkin, S. Lambert, A. Abbott, E. Kendrick, A. Walton, K. Ryder, L. Driscoll, L. Gaines, P. Christensen, O. Heidrich and P. Anderson, *Nature*, 2019, **575**(7781), 75–86.
4 J. Zhu, K. Zeng and L. Li, *Electrochim. Acta*, 2012, **68**, 52–59.
5 C. Tomon, S. Sarawutanukul, N. Phattharasupakun, S. Duangdangchote, P. Chomkhuntod, N. Joraleechanchai, P. Bunyanidhi and M. Sawangphruk, *Commun. Chem.*, 2022, **5**(1), 54.
6 Q. Zheng, K. Shibazaki, T. Ogawa and M. Watanabe, *ACS Sustainable Chem. Eng.*, 2021, **9**(33), 10970–10976.
7 R. Wang, X. Chen, Z. Huang, J. Yang, F. Liu, M. Chu, T. Liu, C. Wang, W. Zhu, S. Li, S. Li, J. Zheng, J. Chen, L. He, L. Jin, F. Pan and Y. Xiao, *Nat. Commun.*, 2021, **12**(1), 3085.
8 X. Xu, Y. Chen, P. Wan, K. Gasem, K. Wang, T. He, H. Adidharma and M. Fan, *Prog. Mater. Sci.*, 2016, **84**, 276–313.
9 X. Lai, P. Xiong and H. Zhong, *Hydrometallurgy*, 2020, **192**, 105252.
10 R. Li, Y. Wang, W. Duan, C. Du, S. Tian, Z. Ren and Z. Zhou, *Desalination*, 2023, **555**, 116543.
11 T. Zhang, Y. Chen, Q. Yu, H. Sun, K. Chen, H. Ye, S. Tang, H. Zhang, P. Li and Q. J. Niu, *Appl. Surf. Sci.*, 2023, **616**, 156434.
12 H. Saravaia, H. Gupta and V. Kulshrestha, *RSC Adv.*, 2016, **6**(108), 106980–106989.
13 G. Zhang, J. Zhang, Y. Zhou, G. Qia, Y. Wud, C. Hai and W. Tang, *Colloids Surf., A*, 2019, **583**, 123950.
14 R. Marthi and Y. R. Smith, *Hydrometallurgy*, 2019, **186**, 115–125.
15 D. Liu, S. Sun and J. Yu, *Chem. Eng. J.*, 2019, **377**, 119825.
16 X. Shang, Z. Liu, W. Ji and H. Li, *Sep. Purif. Technol.*, 2021, **262**, 118294.
17 S. Yang, Y. Wang, H. Pan, P. He and H. Zhou, *Nature*, 2024, **636**(8042), 309–321.
18 D. Weng, H. Duan, Y. Hou, J. Huo, L. Chen, F. Zhang and J. Wang, *Prog. Nat. Sci.:Mater. Int.*, 2020, **30**(2), 139–152.
19 Z. Ji, M. Zhao, J. Yuan, J. Wang, J. Zhou, H. Yin and B. Sun, *Solvent Extr. Ion Exch.*, 2016, **34**(6), 549–557.
20 J. C. Hunter, *J. Solid State Chem.*, 1981, **39**, 142–147.
21 K. Ooi, Y. Miyai and J. Sakakihara, *Langmuir*, 1991, **7**, 1167–1171.
22 T. Hatakeyama, N. L. Okamoto and T. Ichitsubo, *J. Solid State Chem.*, 2022, **305**, 122683.
23 Q. Zhang, S. Li, S. Sun, X. Yin and J. Yu, *Chem. Eng. Sci.*, 2010, **65**(1), 169–173.
24 C. Özgür, *Solid State Ionics*, 2010, **181**(31–32), 1425–1428.
25 Y. Han, H. Kim and J. Park, *Chem. Eng. J.*, 2012, **210**, 482–489.
26 J. Wang, G. Wang, Y. Wang, L. Li, Y. Ma, C. Li and S. Dai, *Ind. Eng. Chem. Res.*, 2020, **59**(29), 13239–13245.
27 L. Wang, C. Meng, M. Han and W. Ma, *J. Colloid Interface Sci.*, 2008, **325**(1), 31–40.
28 D. M. Robinson, Y. B. Go, M. Greenblatt and G. C. Dismukes, *J. Am. Chem. Soc.*, 2010, **132**, 11467–11469.
29 C. M. Ghimbeu, E. Frackowiak, A. Malak-Polaczy and C. Vix-Guterl, *J. Appl. Electrochem.*, 2013, **44**(1), 123–132.
30 J. Yuan, H. Yin, Z. Ji and H. Deng, *Ind. Eng. Chem. Res.*, 2014, **53**(23), 9889–9896.
31 L. Liu, H. Zhang, Y. Zhang, D. Cao and X. Zhao, *Colloids Surf., A*, 2015, **468**, 280–284.
32 T. Oshima, Y. Kadogawa, K. Shiraishi, K. Ohe, S. Nishihama and K. Yoshizuka, *Solvent Extr. Ion Exch.*, 2024, **43**(1), 79–93.
33 C. Xiao, Y. Qiao, T. Wang and Y. Wang, *J. Phys. Chem. C*, 2025, **129**(37), 16918–16926.
34 Z. Zhou, Y. Liu, Z. Tang, J. Xia, H. Jin, J. Zhang, Y. Chen and C. Wang, *Chem. Commun.*, 2023, **59**(26), 3906–3909.
35 K. Ooi, Y. Miyai, S. Katon, H. Maeda and M. Abe, *Chem. Lett.*, 1988, **17**(6), 989–992.
36 H. Ogino and T. Oi, *Sep. Sci. Technol.*, 1996, **31**(9), 1215–1231.
37 Z. Ji, M. Zhao, Y. Zha, J. Liu, J. Peng and J. Yuan, *Solid State Ionics*, 2017, **301**, 116–124.
38 Y. Kong, Y. Takaya, M. Cordova-Udaeta and C. Tokoro, *Sep. Purif. Technol.*, 2023, **322**, 124280.
39 Z. Han, B. Liu, S. Yang, X. Pan and Z. Yan, *J. Chem.*, 2017, **2017**, 1–10.
40 S. Yang, Z. Han, J. Dong, Z. Zheng and X. Pan, *J. Chem.*, 2016, **2016**, 6065019.
41 S. Fukuzaki, *Biocontrol Sci.*, 2006, **11**(4), 147–157.
42 M. Debordea and U. von Gunten, *Water Res.*, 2008, **42**(1–2), 13–51.
43 H. Li, M. Lin, T. Xiao, J. Long, F. Liu, Y. Li, Y. Liu, D. Liao, Z. Chen, P. Zhang, Y. Chen and G. Zhang, *J. Hazard. Mater.*, 2020, **388**, 122016.
44 W. Lv, Z. Wang, X. Zheng, H. Cao, M. He, Y. Zhang, H. Yu and Z. Sun, *ACS Sustainable Chem. Eng.*, 2020, **8**(13), 5165–5174.
45 Y. Yang, X. Meng, H. Cao, X. Lin, C. Liu, Y. Sun, Y. Zhang and Z. Sun, *Green Chem.*, 2018, **20**(13), 3121–3133.
46 M. Córdova-Udaeta, B. Cheng, S. Fuchida, Y. Takaya, K. Oyama and C. Tokoro, *J. Chem. Eng. Jpn.*, 2024, **57**, 2366409.
47 I. Puigdomènech, E. Colàs, M. Grivé, I. Campos and D. García, *Mater. Res. Soc. Symp. Proc.*, 2014, **1665**, 111–116.
48 Q. Jing, J. Zhang, Y. Liu, C. Yang, B. Ma, Y. Chen and C. Wang, *J. Phys. Chem. C*, 2019, **123**(23), 14207–14215.
49 Y. Li, W. Lv, H. Huang, W. Yan, X. Li, P. Ning, H. Cao and Z. Sun, *Green Chem.*, 2021, **23**(17), 6139–6171.
50 A. Manthiram, *Nat. Commun.*, 2020, **11**(1), 1550.
51 J. Ling, C. Karuppiah, S. G. Krishnan, M. V. Reddy, I. I. Misnon, M. H. A. Rahim, C. Yang and R. Jose, *Energy Fuels*, 2021, **35**(13), 10428–10450.
52 M. Y. Saidi, J. Barker and R. Koksbang, *Electrochim. Acta*, 1996, **41**, 199–204.
53 K. Kanamura, H. Naito, T. Yao and Z. Takehara, *J. Mater. Chem.*, 1996, **6**(1), 33–36.
54 S. Martinez, I. Sobrados, D. Tonti, J. M. Amarilla and J. Sanz, *Phys. Chem. Chem. Phys.*, 2014, **16**(7), 3282–3291.
55 G. Pistoia and G. Wang, *Solid State Ionics*, 1993, **66**, 135–142.

56 T. Ohzuku, M. Kitagawa and T. Hirai, *J. Electrochem. Soc.*, 1990, **137**(3), 769–775.
57 Y. Lee, F. Wang, S. Mukerjee, J. McBreen and C. P. Grey, *J. Electrochem. Soc.*, 2000, **147**, 803–812.
58 M. Murakami, S. Shimizu, Y. Noda, K. Takegoshi, H. Arai, Y. Uchimoto and Z. Ogumi, *Electrochim. Acta*, 2014, **147**, 540–544.
59 J. Wang, R. Yunus, J. Li, P. Li, P. Zhang and J. Kim, *Appl. Surf. Sci.*, 2015, **357**, 787–794.
60 V. P. Santos, M. F. R. Pereira, J. J. M. Órfão and J. L. Figueiredo, *Appl. Catal., B*, 2009, **88**(3–4), 550–556.
61 X. Wang, X. Zhang, L. Dai, H. Guo, P. Shi, Y. Min and Q. Xu, *ACS Sustainable Chem. Eng.*, 2020, **8**(30), 11337–11347.
62 F. Marchini, D. Rubi, M. del Pozo, F. J. Williams and E. J. Calvo, *J. Phys. Chem. C*, 2016, **120**(29), 15875–15883.
63 F. Marchini, E. J. Calvo and F. J. Williams, *Electrochim. Acta*, 2018, **269**, 706–713.
64 Q. Feng, Y. Miyai, H. Kanoh and K. Ooi, *Langmuir*, 1992, **8**(7), 1861–1867.
65 E. Billy, M. Joulié, R. Laucournet, A. Boulineau, E. De Vito and D. Meyer, *ACS Appl. Mater. Interfaces*, 2018, **10**(19), 16424–16435.
66 H. Zhu, J. Luo, H. Yang, J. Liang, G. Rao, J. Li and Z. Du, *J. Phys. Chem. C*, 2008, **112**, 17089–17094.
67 L. A. Limjuco, G. M. Nisola, C. P. Lawagon, S. Lee, J. G. Seo, H. Kim and W. Chung, *Colloids Surf., A*, 2016, **504**, 267–279.